A comparison of modelled ice thickness and volume across the entire Antarctic Peninsula region

Jonathan L. Carrivick[1*], Bethan J. Davies[2], William H.M. James[1], Malcolm McMillan[3], Neil F. Glasser[4]

[1]School of Geography and water@leeds, University of Leeds, Woodhouse Lane, Leeds, West Yorkshire, LS2 9JT, UK
[2]Centre for Quaternary Research, Department of Geography, Royal Holloway University of London, TW20 0EX, UK
[3]School of Earth and Environment, University of Leeds, Woodhouse Lane, Leeds, West Yorkshire, LS2 9JT, UK
[4]Department of Geography and Earth Sciences, Aberystwyth University, Wales, SY23 3DB, UK

*Correspondence to:
Dr. Jonathan Carrivick,
Email: j.l.carrivick@leeds.ac.uk
Tel.: 0113 343 3324

ABSTRACT

Understanding Antarctic Peninsula glacier evolution requires distributed ice thickness and subglacial topography. To date, 80 % of the Antarctic Peninsula mainland ice volume has only been determined at low-resolution (1 km post spacing) and the distributed ice thickness of glaciers on surrounding islands has never been quantified. In this study we applied a perfect plasticity model, selected for its simplicity, low data requirements and minimal parameterization, to estimate glacier thickness, subglacial topography and ice volume for the entire Antarctic Peninsula region. We compared the output of this simple model to that of a more sophisticated but spatially-restricted model and also to the spatially-coarse but more extensive Bedmap2 dataset. The simple model produced mean differences of 1.4 m (std. dev. 243 m) in comparison with the more sophisticated approach for the mountainous parts of the Peninsula. It produced similar volumes for tidewater glaciers but gave unrealistic ice thickness around grounding lines. Ice thickness across low gradient plateau surfaces are mis-represented by a perfect plasticity model and thus for the southern part of the Peninsula only regional ice volume can be approximated by our model. Overall, with consideration of ice situated below sea level, model results suggest that Trinity Peninsula, Graham Land, the part of Palmer Land north of 74°S and all glaciers on islands contain an ice mass of ~200,300 Gt, with sea level equivalent of 553 mm (± 11.6 mm). Of this total 8 % is from glaciers on islands, 70 % of which is from Alexander Island.

KEYWORDS glacier; Antarctica, sea level

INTRODUCTION

The Antarctic Peninsula has been one of the most rapidly warming areas on Earth (Morris and Vaughan, 2003; Turner et al., 2009, 2013). The effects of this warming, together with oceanic forcings, have been recognised in the dramatic collapse of multiple ice shelves (Scambos et al., 2003; Skvarca and DeAngelis, 2003; Paolo et al., 2015; Cook and Vaughan, 2010) and in widespread glacier thinning (Pritchard et al., 2009; Kunz et al., 2012), acceleration (Pritchard and Vaughan, 2007) and recession (Cook et al., 2005, 2014; Glasser et al., 2011; Ivins et al., 2011). These glacier changes are a major reason why the Antarctic Peninsula region is considered to be vulnerable to climate change (Barrand et al., 2013; Davies et al., 2014; O'Cofaigh et al., 2014; Pfeffer et al., 2014). Warming across the Antarctic Peninsula in the 21st century has not been significant (Turner et al., 2016).

The Antarctic Peninsula ice sheet and glaciers on surrounding islands have been estimated to presently contribute between 4 % and 16 % of the observed global sea level rise (SLR) (c.f. Hock et al., 2009; Shepherd et al., 2012; Gardner et al., 2013). A small amount of this SLR contribution is from calving of tidewater glaciers and tabular icebergs, but also from ice shelf basal melt (e.g. Rignot et al., 2013; Depoorter et al., 2013) due to the density difference between water and ice. Snow and ice melt on the Antarctic Peninsula surface mostly refreezes within the snowpack (van Wessem, et al., 2016) and on ice shelves contributes to numerous and extensive surface ponds (Kingslake et al., 2017). Nonetheless, the importance of surface and basal melt to ice mass loss (Hock et al., 2009; Radic and Hock, 2011; Pritchard et al., 2012) is likely to persist and possibly increase in the next decades to centuries (Golledge et al., 2015). It is therefore important to estimate glacier ice thickness and bed topography across the entire Antarctic Peninsula region, for (i) baseline data useful for monitoring of these ice-mass changes, (ii) understanding potential local meltwater contributions via glacier hypsometry and likely equilibrium line altitude (ELA) rises, (iii) revealing subglacial topography that will become exposed as glaciers diminish, (iv) comparing ice mass loss observed from gravimetric and satellite data (e.g., Ivins et al. 2011), (v) ice flux calculations at grounding lines, and thus investigating tidewater glacier stability, e.g. due to retrograde bed slopes (Schoof, 2007) and sensitivity to ocean forcing. Furthermore, because the Antarctic Peninsula comprises several different morpho-climatic sub-regions (Barrand et al., 2013a; Cook et al., 2014), potential sea level contributions should be estimated per glacier.

Ice thickness across the entire Antarctic Peninsula region is poorly known and different methods are currently used to estimate ice thickness. Ice flow model-based approaches have the advantage of accounting for mass conservation (e.g. Morlighem et al., 2011) but can be relatively computationally expensive to run over large domains. In an approach that is not technically mass conserving due to the use of a correction procedure, Huss and Farinotti (2014) used an ice flow model driven by estimated mass balance parameters to calculate that the sea level equivalent of the Antarctic Peninsula north of 70°S is 69 ± 5 mm. However, they did not include any of the mainland glaciers between 70°S and 74°S, which account for ~ 60 % of the Antarctic Peninsula region glacierised area. They also did not closely analyse the distributed ice thickness, which they posted at 100 m resolution, and volume on the surrounding islands even though these are amongst the most rapidly changing glaciers within the whole Antarctic Peninsula region (Davies et al., 2012). They corrected their model to ice thickness measured at points along transects flown by Operation Ice-Bridge (2016) airborne radar, but these flight lines are widely spaced and often with only one longitudinal pass per glacier. Huber et al. (2017) have completed a glacier inventory of the Antarctic Peninsula, including ice thickness and volume per glacier which they derived from Huss and Farinotti's (2014) data, but again only for part of the peninsula north of 70 ^{o}S, i.e. Graham Land.

The only complete coverage of ice thickness across the entire Antarctic Peninsula is that of the Bedmap2 dataset (Fretwell et al., 2013), which was compiled from multiple data sources and interpolated to provide a seamless though relatively coarse resolution gridded product of 1 km. Observational ice thickness estimation methods such as Bedmap2 have the advantage that they are tuned to best-fit ice thickness and bed data, but they are highly reliant upon interpolation where data are sparse. Indeed, the 1 km grid of Bedmap2 does not represent the typically mountainous subglacial terrain of the Antarctic Peninsula very well (cf. Huss and Farinotti, 2014).

Therefore in this study we implement an alternative approach to ice thickness estimation which is independent of bed data and which is computationally simple and fast. Specifically, we use a perfect plasticity model to calculate subglacial bed topography and distributed ice thickness for all individual glaciers in the Antarctic Peninsula region between 60°S and 74°S, including all of the mainland ice sheet and all glaciers on surrounding islands. We report our model results relative to these other (model-based and observational) methods to compare the results.

STUDY AREA

The Antarctic Peninsula stretches from the northern tip of the Trinity Peninsula, including the South Shetland and South Orkney islands, to glacier drainage basins in Palmer Land north of 74°S. The entire Antarctic Peninsula is ~1500 km long and varies in width from ~25 km wide across the Trinity Peninsula to 230 km wide across the southern part of Graham Land and to ~ 430 km wide across Palmer Land near the southern part of Alexander Island (Fig. 1). Between 63°S and 67°S, the Peninsula is characterised by a plateau with ice surface elevations up to 2000 m.asl. Further south to 74°S, the plateau rises to >2500 m.asl. This topography means that the Antarctic Peninsula is subjected to subpolar climates in the north and far colder conditions in the south. It is also subject to strongly contrasting oceanographic and meteorological conditions across the east-west gradient (Domack et al., 2006), with large amounts of snow reaching the western Peninsula as a result of the prevailing Westerlies. The glaciers on the western Peninsula therefore experience high accumulation and have low equilibrium line altitudes (Domack et al., 2006; Davies et al., 2012), whereas glaciers on the colder, drier eastern side of the Peninsula have higher equilibrium line altitudes.

The Antarctic Peninsula is surrounded by many islands, including James Ross Island in the northeast, the South Shetland Islands in the northwest, and Alexander Island in the southwest (Fig. 1). Significant ice shelves include Larsen C, with an area of 50,837 km^2 in 2008, Larsen D (22,602 km^2), George VI (24,045 km^2) and Wilkins (11,144 km^2) (Cook and Vaughan, 2010), although there are numerous smaller ice shelves and floating ice tongues surrounding most of the coastline (Fig. 1). Between 63°S and 70°S, over 96 % of the mainland is ice covered (Cook et al., 2014) and between 70°S and 74°S virtually all of the land is ice covered.

Summer air temperatures on the Antarctic Peninsula frequently reach > 0°C, meaning that widespread summer surface snowmelt occurs (Barrand et al., 2013b). The Antarctic Peninsula has warmed significantly since the early 1950s with (i) warming trends on the western and northern parts; Faraday/Vernadsky station (65.4°S) on the western Peninsula warmed at +0.54 °C per decade from 1951 to 2011 with fewer extreme cold winters, and Orcadas (South Orkney Islands) has warmed at +0.21°C per decade since 1904 (Turner et al., 2013); and (ii) the greatest increase in positive degree days experienced in the north-east at Esperanza and at Marambio (see Barrand et al., 2013). There has been a climate warming hiatus in the peninsula region since the early 2000s (Turner et al. 2016; Oliva et al. 2017).

The atmospheric warming has predominantly been attributed to a local strengthening of the circumpolar westerly winds, driven by changes in the summer Southern Hemisphere Annular Mode (Martinson et al., 2008; Turner et al., 2013). It has also produced an increased number of, and intensified, foehn winds, which are strongly associated with surface melting across the Antarctic Peninsula ice sheet and ice shelves (van den Broeke, 2005; Cape et al., 2015). Consequently ice surface melting has increased on the Antarctic Peninsula since the 1950s with both longer melt seasons and more positive degree days (Barrand et al., 2013b). Long-term air temperature series are strongly correlated between stations on either side of the Antarctic Peninsula indicating that these trends are pervasive across Graham Land. Rising air temperatures have been implicated in ice-shelf collapse (Turner et al., 2013; Cook and Vaughan, 2010) and widespread glacier acceleration (Pritchard and Vaughan, 2007) and recession (Davies et al., 2012). Additionally, retreat of tidewater glacier termini and glacier thinning on the western side of the Antarctic Peninsula is strongly impacted by ocean warming (Martinson et al., 2008; Schmidtko et al. 2014; Wouters et al. 2015; Cook et al., 2016).

DATASETS AND METHODOLOGY

This study applied the VOLTA model which is a perfect-plasticity approach to modelling ice thickness, bed elevation and glacier volume and which is available for download via James and Carrivick (2016).

This model is attractive for application to multiple mountain glaciers over large spatial scales because it is minimalist in its data requirements; it requires only glacier outlines and an ice surface DEM for input, and because it is computationally efficient. The VOLTA model is implemented as an ArcGIS (version 10.2 and more recent) tool for ease of use and all major parameters can be manually edited.

Whilst this type of model performs well for deriving approximations of ice thickness at land-terminating mountain glaciers (James and Carrivick, 2016; Carrivick et al., 2016), and has been applied to the mountain glaciers, ice caps and the major ice fields of Patagonia and southern South America (Carrivick et al., 2016), it has not yet been assessed for deriving ice thicknesses across tidewater glaciers, nor for glaciers flowing into an ice shelf. This is because of the inappropriateness of this type of model for both calving tidewater glaciers and ice shelf tributary glaciers which are not in steady state. In particular they have significant longitudinal stresses that are sensitive to (de)buttressing (e.g. Vieli and Nick, 2011), and they often have rapidly-expanding flow in floating parts, for example in feeding ice shelves. Across the entirety of the Antarctic Peninsula, 17 % of the glaciers north of 70^{o}S and 63 % of the glaciers south of 70^{o}S are marine-terminating, as we have determined by identifying geospatial intersections of our

outlines with the grounding lines mapped by Rignot et al. (2011). However, Huber et al. (2017) reported that 63 % are tidewater glaciers and they based that calculation on the Landsat Image Mosaic of Antarctica (LIMA) by Bindschadler et al. (2008) and the fact that many glacier termini elevations correspond to sea level in the Cook et al. (2012) DEM. Ice shelf tributary glaciers drain 35% of the glaciated area (Huber et al. 2017). We therefore seek to understand to what extent ice thickness across the entire Antarctic Peninsula can reasonably be estimated by using a simple perfect plasticity model and so have herein made a comparison of our ice thickness modelling results with results from other existing ice thickness models, including at grounding lines, and specifically targeting the few land-terminating and tidewater glaciers on the Antarctic Peninsula where field-measured ice thickness data are available.

Our glacier outlines combined those available for surrounding islands (Bliss et al., 2013) with glacier outlines on the Trinity Peninsula (Davies et al., 2012) and drainage basins of Graham Land (Cook et al., 2014). The outlines and drainage basins identify nunataks and thus could be masked out so that glacier area could be calculated separately from drainage basin area. The outlines were clipped so as not to extend beyond the grounding line(s) identified for all Antarctic Peninsula tidewater glaciers by Rignot et al. (2011) and so in this study we do not consider any floating ice. In total these data comprised 1781 outlines. Major glacierised regions were discriminated spatially following British Antarctic Survey (2005) name conventions for the mainland and the surrounding islands were grouped according to their geographic position relative to these mainland regions (Fig. 1, Table 1).

In this study the ice surface DEM of Cook et al. (2012) was used for regions north of 70^{o}S. To compute ice-surface elevation south of 70°S we used CryoSat-2 interferometric mode altimeter measurements. CryoSat-2 elevation data were taken from the Baseline-C distribution and spanned the period 2011-2014 inclusive. Using these data, we generated a continuous DEM by (i) median-gridding the data at 5 km resolution, (ii) removing noisy or topographically-complex cells where the median absolute deviation of measurements exceeded 50 m, and then (iii) posting to a 100 m grid using bilinear interpolation. Ice surface DEMs were projected into a Cartesian coordinate system and clipped to the spatial extent of the glacier outlines for efficiency when running the model. We compared our centreline point ice thickness values to the ice thickness points of Operation Ice-Bridge (2016): data from http://nsidc.org/icebridge/portal/, and we compared our gridded ice thickness with the gridded data in the Bedmap2 dataset of Fretwell et al. (2013), and with that of Huss and Farinotti (2014). While Bedmap2 is provided at a nominal 1 km resolution, the actual resolution for the peninsula region is much coarser. Huss and Faronotti's dataset is at 100 m resolution.

198

199 ***Glacier centrelines***

200 Identification of glacier ice surface flow trajectories requires fully distributed velocity fields, which are
201 available for Antarctica on a 300 m grid from Rignot et al. (2011). Using these flow trajectories as a
202 guide, because they only provide ~70% coverage over the Antarctic Peninsula region, we manually
203 digitized glacier centrelines from the middle of each glacier terminus up-glacier and approximately
204 midway between and parallel to the lateral margins of any glacier ablation tongue, and thence towards
205 any prominent saddles or cols on cirque headwalls or on ice divides. Where ice divides were
206 ambiguous we inverted the DEM and then ran a hydrological routing function in ArcGIS 10.4, which is
207 normally used to delineate valley floor flow paths but in this case identified 'ridge lines'. The exact
208 position of our centrelines, especially south of 70ºS is thus partly a function of the quality of the DEM.
209 We used the ridgeline analysis only as a guide and we performed a sensitivity test on the number and
210 position of centrelines as will be shown below.

211

212 As described by James and Carrivick (2016), a single centreline may not be suitable if a glacier is of
213 complex geometry due to multiple tributaries or cirques. Whilst the lack of a secondary tributary
214 centreline is the main issue, the initial centreline is also laterally deflected where the perpendicular
215 traverses are elongated as they continue into the secondary tributary. To overcome these issues, an
216 upstream area approach was used to delineate separate tributaries. Iteratively working down the initial
217 centreline, upstream area is calculated. Total area steadily increased down-centreline, but a marked
218 (rate of) increase occurs when a new tributary enters. VOLTA calculates area at an interval equal to 1
219 % of centreline length with a new tributary identified if area increases by > 30 % between successive
220 points. Furthermore, we stipulate for computational efficiency that any new tributary must also have an
221 area of at least 20 % of the total for any glacier.

222

223 ***Calculating ice thickness at points along the centreline***

224 Ice thickness *h* of mountain glaciers can be estimated from a glacier surface slope by:

225

227 $$h = \frac{\tau_b}{fpg\ tan\ \alpha}$$

226

228 where , τ_b is basal shear stress, a shape factor *f* is required to account for valley sides supporting part of
229 the weight of the glacier, ρ is ice density, g is the gravitational constant and α is the surface slope angle.
230 Since the VOLTA model is published (James and Carrivick, 2016) we simply cover the most salient

231 points here. These points firstly concern the basic operation of the model, and secondly the question of
232 how to recognize the uncertainty introduced by using this sort of model on Antarctic Peninsula glaciers.
233 The Peninsula includes tidewater glaciers and wide lobate outlet type glaciers and thus these glaciers
234 can have a completely different morphology (due to different processes) to land-terminating mountain
235 glaciers.
236
237 Basal shear stress, $\tau_{b,}$ is variable between individual glaciers due mainly to basal water pressure, ice
238 viscosity and subglacial sediment deformation. For ice thickness estimations such as those within in
239 this study, τ_b does not have to be varied longitudinally for an individual glacier as a constant value can
240 reproduce accurate thickness estimates along the length of a centreline (Li et al., 2012). Previous
241 studies have used an empirical relationship between altitudinal extent and τ_b that was developed by
242 Haeberli and Hoelzle (1995) but the relationship is weak ($r^2 = 0.44$) and Linsbauer et al. (2012)
243 reckoned an uncertainty of up to ± 45% using this method. Therefore in this study we employ a
244 relationship established by Driedger and Kennard (1986a), using area and slope in an elevation band
245 approach:

246 $$\tau_b = 2.7 \cdot 10^4 \sum_{i=1}^{n} \left(\frac{A_i}{\cos \alpha_i}\right)^{0.106}$$

247 where the elevation band area (A_i) is in m^2 and τ_b is in Pa. This method was tested by Driedger and
248 Kennard (1986b) as part of a volume estimation study and they found a standard deviation of error of 5
249 % when comparing modelled with measured volumes. We calculated A_i and $\cos\alpha_i$ over 200 m ice-
250 surface elevation bands to produce glacier specific average τ_b values that were consequently applied to
251 each centreline point.
252
253 We calculated *h* at points spaced 100 m apart on all centrelines where that spacing was selected partly
254 with respect to our 100 m posting to combine the ice surface DEMs and partly due to the spatial
255 coverage of this study and a desire to maintain computational efficiency. Whilst *f* has been incorporated
256 as a constant (usually 0.8 cf. Nye et al., 1965; e.g. Linsbauer et al., 2012), we adopted the practice of Li
257 et al. (2012) who developed a more physically realistic method to dynamically adjust *f* depending on
258 the local width of a glacier. In detail, Li et al. (2012) estimated ice thickness perpendicular to the ice
259 surface but in this study we are dealing with GIS-analysed glacier geometry so to consider 'vertical' ice
260 thickness, h, i.e. that perpendicular to a horizontal x-axis we re-write the Li et al. (2012) equation as:
261

$$h = \frac{0.9\, w\left(\frac{\tau_B}{pg \tan \alpha}\right)}{0.9\, w - \left(\frac{\tau_B}{pg \tan \alpha}\right)}$$

where w is half the glacier width at the specified point on a centreline.

We then implemented an automatic check for erroneous h values in the vicinity of nunataks and tributary confluences (cf. Li et al. 2012) by: (i) checking if the perpendicular 'width' line intersected another centreline and (ii) cross checking if the resulting f value (Eq. 1) is realistic (> 0.445, equal to a half width to centreline thickness ratio of 1: cf. Nye, 1965). At points where either of these conditions were met, h was calculated using Eq. 1, with f set to that of the average of all points on the same tributary.

Ice thickness, h, will tend to infinity as surface slope tends to zero, meaning h may be overestimated in regions of flatter ice surface (Li et al., 2012; Farinotti et al., 2009). In this study a 'minimum slope threshold' α_0 of 1.5° was used to re-assign any lower slope values to that minimum value. We note that Farinotti et al. (2009) used 5° and Li et al. (2012) used 4°, but since 49 % of the ice surface across the Antarctic Peninsula (5 % of area outside Palmer Land; 95 % of area within Palmer Land) is 2° or less this was too high for application to the glaciers of the Antarctic Peninsula. Additionally, the 'low slope' parts of ice surfaces are situated either within the trunks of the major outlet glaciers outside of Palmer Land, or across the southern Antarctic Peninsula plateau of Palmer Land. Approx. 47 % of the ice surface in this study is < 1.5°.

Interpolating distributed ice thickness and bed topography

Distributed ice thickness was interpolated from the centreline points across each glacier using the ANUDEM 5.3 interpolation routine (Hutchinson et al., 1989). ANUDEM generates preferably concave shaped landforms, thus mimicking the typical parabolic shape of (idealised) glacier beds (Linsbauer et al., 2012). It is commonly applied to estimating bed topography of both mountain valley glaciers (Farinotti et al., 2009; Linsbauer et al., 2012; Li et al., 2012; Fischer and Kuhn, 2013), to ice caps and ice fields (Carrivick et al., 2016) and to ice sheets, such as within the Antarctica Bedmap2 dataset (Fretwell et al., 2013). Interpolations of ice thickness through ice divides was achieved simply by 'dissolving' (i.e. removing) those parts of glacier outlines that were in contact with each other. If glaciers were exceptionally wide, such as in the southern part of the Peninsula, we digitized multiple

sub-parallel centrelines within a single glacier outline and this served to accommodate applying the VOLTA model to large low-gradient lobate and coalescing outlet glaciers that are typical of the southern part of the Antarctic Peninsula (Fig. 2).

Once thickness *h* for each grid cell in each glacier had been interpolated, total volume *V* was calculated:

$$V = \sum (c^2 h)$$

where *c* is the grid cell size.

Uncertainty estimates

James and Carrivick (2016) compared modelled glacier volume to that derived from field measurements of (individual) (land-terminating) valley glaciers around the world, and found worst-case 26.5 % underestimates and 16.6 % overestimates. Median deviations of modelled to measured ice thickness on a cell by cell basis were ~ 10% (James and Carrivick, 2016 their Fig. 9 and their Table 2). For comparison, uncertainties for volume-scaling approaches range from 30 % for large samples to 40 % when considering smaller (~ 200) samples Farinotti and Huss, 2013; Bahr et al., 2014a, b). In this study, model error comes from individual model parameters, from the perfect plasticity assumption and uncertainty comes from the spatial interpolation from centreline thicknesses to glacier-wide thickness. James and Carrivick (2016) compared centreline modelled ice thickness with ice thickness from field radar measurements on alpine glaciers around the world and found differences < 11 %. They also found that the modelled volume of large glaciers was least sensitive to model parameters basal shear stress, slope averaging distance, minimum slope threshold and effective width slope threshold, in comparison to the sensitivity of small glaciers to these parameters Across the entire Antarctic Peninsula mainland and surrounding islands 82 % of all glaciers are > 2 km^2 (and 63 % are > 5 km^2) so at least in regard of their size should be well-suited to application of this model.

In this study we firstly compared our ice thickness results to independent ground penetrating radar (GPR) measurements made by Engel et al. (2012) on IJR-45 (a land-terminating valley glacier) and across the Davies Dome ice cap, both on the Ulu Peninsula of James Ross Island. Our uncertainty analysis was informed by the work on mountain glaciers of James and Carrivick (2016), but also took advantage of the aforementioned GPR data, which is not included in Bedmap2. Modelled-measured comparisons were made along glacier centrelines and on flow-perpendicular transects where GPR-

326 measurements have been made and produced median modelled-measured differences of 32 m and a
327 maximum of 62 m (Fig. 3). On the basis of these comparisons we herein report modelled ice thickness
328 on land-terminating valley glaciers with uncertainty of ± 31 % and glacier volume with uncertainty of ±
329 20 % but note that these uncertainties are both worst case estimates. For land-terminating ice caps the
330 uncertainty in ice thickness is up to 45 % (Fig. 3) due to the shallow gradient ice surfaces but ice
331 volume uncertainty is the same at 20 % because over- and under-estimates of ice thickness tend to
332 cancel each other out.
333
334 Secondly, to gain an estimate of the uncertainty in our model for the distributed ice thickness in the
335 vicinity of grounding lines, we compared our ice thickness results with those of Farinotti et al. (2013)
336 for Flask Glacier, and with those of Farinotti et al., (2014) for Starbuck Glacier. Both datasets were
337 incorporated by Huss and Farinotti (2014) in their study to correct their model. These comparisons of
338 model results (Fig. 4) show that our model has considerable error in the vicinity of a grounding line,
339 because it tends towards zero ice thickness at non-adjacent glacier boundaries as would be the case for
340 land-terminating glaciers. However, that effect does not propagate more than a few kilometres up-
341 glacier and so has only a spatially-restricted effect on distributed ice thickness, and a negligible effect
342 on the magnitude of modelled ice volume (Fig. 4).
343
344 It is apparent that for the glaciers on the Antarctic Peninsula bounded by steeply sided mountain slopes
345 and thus of an alpine character, our model can replicate the ice thickness suggested by Huss and
346 Farinotti, as evidenced by the general spatial pattern of ice thickness and by a histogram of absolute
347 differences between the two models where the mean difference is 1.4 m, the standard deviation of the
348 differences 676 and -953m, respectively (Fig. 4). On the basis of these comparisons of our modelled ice
349 thickness for tidewater glaciers with that measured, we herein report modelled ice thickness across
350 tidewater glaciers with a mean uncertainty of ± 16 % and glacier volume with a mean uncertainty of ±
351 20 %. We assume that these uncertainty estimates are representative of the surrounding islands, the
352 Trinity Peninsula and for Graham Land due to the similar mountain topography in those regions.
353
354 Thirdly, we considered the utility of our model across Palmer Land, where interpolation distances
355 (glacier widths) are much larger, where ice surface slopes are very low and where the only independent
356 ice thickness measurements available are those of Operation Ice-Bridge. Manually moving (laterally) our
357 sub-parallel multiple centrelines by up to 5 km had a negligible effect of the overall pattern of ice

thickness or on individual glacier volume. However, changing the number of sub-parallel centerlines did have a significant effect and for this reason we located sub-parallel centrelines (Fig. 2A) where thicker parts of the glaciers as depicted in the Bedmap2 dataset reached the grounding line (Fig. 2B). Our results reported below include a cross-over analysis of our centreline ice thickness points with ice thickness points derived from airborne radar surveys.

Spatial and statistical analysis

Zonal statistics per glacier, per major glacial region and per major glacier catchment were extracted from ice-surface elevation, ice thickness and subglacial bed topography grids. Areas with bed elevations below sea level were automatically extracted via a binary reclassification of bed topography [> 0 m.asl = 0; < 0 m.asl = 1], conversion of the '1' values in this grid to polygons, and then zonal analysis of bed topography per polygon zone. The part of ice below sea level in each grid cell column was excluded from estimates of potential sea level rise. Overdeepenings were automatically extracted from bed topography by 'filling sinks' in the bed topography and analysed in the same manner as for bed elevations.

Conversion of ice thickness to potential sea level rise

As snowfall and temperature are not uniform across the Peninsula, the thickness of the snow and firn layer is not uniform and therefore gridded 'ice column' densities are spatially variable. However, quantifying this spatial variation is not trivial and is poorly constrained by field observations. We therefore converted our ice volumes to a mass by assuming a mean density of 852 $kg.m^{-3}$ to account for the fact that each grid cell is not just a thickness of ice but also with some significant depth of snow and a firn layer. The firn layer is especially prominent in Palmer Land (Huss, 2013; van Wessem, 2016), according to the modelling by Ligtenberg et al. (2011) using a firn densification model that included liquid water processes (meltwater percolation, retention and refreezing), that was tuned to fit depth-density observations, and that was driven by RACMO at 5.5 km resolution. This mean density is the same value as used by Huss and Farinotti (2014) for the mountainous northern part of the Antarctica Peninsula. Lower density firn layers are thickest on high dry plateau (Ligtenberg et al;., 2011) but it is also in those places, especially Palmer Land, that overall ice thickness is greatest and so mean (ice column) density is probably not to dissimilar to the single global value we use. The mass of ice was converted to a sea level equivalent (SLE) using an ocean area of 3.618×10^8 km^2. Our SLE calculations are not very sensitive to the choice of density value; changing the mean density from 852 to 900 $kg.m^{-3}$ with a volume of 100,000 km^2 produces an increase in SLE of 13 mm.

RESULTS

Our modelled ice thickness grid cell values fall into two groups; those computed on glacier centrelines using the perfect plasticity assumption, and those interpolated between the centrelines and the glacier perimeter. A cross-over analysis of our modelled ice thickness points on our centrelines and the closest Operation Ice-Bridge (OIB) (2016) airborne radar ice thickness points (if within 500 m) gives an r^2 value of 0.41 (Fig. 5A). This is better than the correlation between our ice thickness points and Bedmap2 ice thickness values (r^2 = 0.38; Fig. 5B). But, it is important to realise that (i) Bedmap2 was generated by interpolating from the OIB (2016) points, although the interpolation routine did not preserve the original thickness values, and (ii) Huss and Farinotti (2014) adjusted their model to best-fit the OIB point ice thickness values. It is therefore promising that whilst our model centreline point ice thickness values have a weak agreement with Bedmap2 ice thickness grid values (r^2 = 0.38: Fig. 5B), there is a moderately high correlation between our model centreline point ice thicknesses and the corresponding grid cell values of ice thickness by Huss and Farinotti (2014) (r^2 = 0.58: Fig. 5C).

Unfortunately, the applicability of our model across Palmer Land is very limited due to the extensive shallow gradient ice surface slopes. Our examination of 'cross overs' of our centreline ice thickness estimates with OIB ice thickness points on a very big and very low gradient glacier in Palmer Land shows that 'minimum slope threshold' α_0 below 1.5° (a value of 4 is typically for mountain glacier applications of perfect plasticity models) are necessary to obtain any ice thickness estimate at all, and even that estimate is unrealistic with over- and under-estimates (relative to Bedmap2) > 100 % possible (Fig. 6).

The spatial pattern of the difference in our modelled ice thickness with that of the nearest (if within 500 m) OIB point ice thickness is mapped in Figure 7 and this pattern is dominated by greater differences south of 70°S, illustrating the effects of (i) a poorer ability to compare our modelled ice thickness on centreline points with OIB points due to much larger glaciers with more sparse centrelines (and more sparse OIB lines) and thus with greater distances from a centreline to an OIB point, (ii) more realistic at-a-point ice thickness estimates in steeper mountainous topography (James and Carrivick, 2016) than over broad low-relief ice sheet plateau areas (Figure 7; e.g. Carrivick et al., 2016).

Spatially, the pattern of ice thickness from our model, Bedmap2 (Fretwell et al., 2013) and Huss and Farinotti (2014) is similar (Fig. 8A), but some important discrepancies in the ice thickness modelled in each case must be noted. Our ice thickness grid has the same high spatial sampling (100 m) as Huss

and Farinotti (2014) and resolves the same subglacial mountainous topography (inset of Fig. 8A). However, our ice thickness is apparently too great along the interior of the northern Antarctic Peninsula (Fig. 8A, B, C). In the region south of 70°S and on the surrounding islands our modelled pattern of ice thickness generally agrees with that of Bedmap2 (Fig. 8A; Table 2), but appears smoother primarily due to the different DEMs used to derive the Bedmap2 model and our model.

The most notable discrepancies in the models are thicker ice modelled in this study on Adelaide Island and on Alexander Island than in Bedmap2, and thicker ice modelled in this study in the southern part of Graham Land than in Bedmap2 or in Huss and Farinotti (2014) (Fig. 8A; Table 2). In western Palmer Land our model estimates ice thickness that is up to several times that of Bedmap2, which is disconcerting given that Bedmap2 was fitted to OIB data. The effect of manually drawn multiple sub-parallel centrelines is regrettably evident in the ice thickness grid across Palmer Land (Fig. 2). We therefore contend that whilst our model is unsuitable for estimating distributed ice thickness across the extensive shallow gradient glaciers of Palmer Land, with caution estimates of regional ice volume can be made.

The results of this study and the model of Huss and Farinotti both suggest thicker ice in the mountainous subglacial troughs than the Bedmap2 dataset indicates. In some instances these differences are large; up to ± 1000 m (Fig. 8B, Fig. 5). However, Table 2 shows that when region-by-region statistics are calculated the relative over- or under-estimation by any of the three models varies between major regions. Our predicted ice thicknesses across Palmer Land have a spatial pattern that agrees with Bedmap2 across the eastern side than the western side of the Peninsula (Fig. 8B). Overall, the ice thickness modelled in this study tends to be over-estimated compared to Bedmap2 (Fig. 9A), and tends to be lower than modelled by Huss and Farinotti (2014) (Fig. 9B). The ice thickness of Huss and Farinotti tends to be thicker than in Bedmap2 (Fig. 9C). If spatial pattern (Fig. 8) and grid cell values (Fig. 9) are compared then our modelled ice thickness has greater agreement with the modelled ice thickness of Huss and Farinotti (2014) than with those of Bedmap2. That general agreement is remarkable given the number (‘count’ in Fig. 9) of grid cells being compared between our study and that of Huss and Farinotti. Our modelled subglacial topography below sea level has a spatial pattern very similar to that of Huss and Farinotti (2014) but that pattern compares less well with the Bedmap2 (Fretwell et al., 2013) dataset (Fig. 10). The parts of glaciers below sea level in red in Figure 10 will have an impact on sea level because of the density difference between ice and water and so if (all) that ice were removed and would raise sea level (by a maximum of) ~ 14 mm.

Our results indicate an ice volume on the mainland Antarctic Peninsula that is typically twice that per major region than that provided by Bedmap2, except for 'PL-west' where our model suggests a similar total ice volume reported in Bedmap2, and 'PL-east' where our modelled ice volume is a 20 % under-estimate in comparison with Bedmap2. On surrounding islands our modelled ice volume is on average 50 % more than Bedmap2. There is great discrepancy between our modelled ice volume below sea level with that of Bedmap2 with the greatest proportional differences in the region 'TP-east' (Table 3).

For mainland regions with comparable coverage; namely TP-west, TP-east, GL-west and GL-east, our modelled volumes are 1.5 times more than those by Huss and Farinotti (Table 3). For surrounding islands our modelled volume(s) are comparable to Huss and Farinotti's (2014) results for most regions but 'C-west' is very different (Table 3) due to a more limited spatial coverage in their study. For zones with complete coverage, our volume(s) below sea level are typically three times that modelled by Huss and Farinotti for mainland regions and four times that for surrounding island regions (Table 3).

These discrepancies in spatial coverage, spatial resolution and method between the three models result in estimates of sea level equivalent (SLE) ranging from 35 mm to 715 mm for the Antarctic Peninsula mainland, and from 6 mm to 55 mm for the surrounding islands (Table 3). The estimated SLE calculated by our simple model is 71 % and 84 % for the mainland and for the surrounding island regions, respectively, of that suggested by the Bedmap2 data. Our estimates of SLE agree well with those of Huss and Farinotti (2014) on a region-by-region basis, the biggest difference being 30 % (27 mm versus 19 mm) for region GL-east (Table 3).

The spatial pattern of SLE per major region determined in this study emphasises the importance of including Palmer Land and Alexander Island (Fig. 11A) in SLE estimates. Were they to melt entirely, Trinity Peninsula could contribute 4 mm ± 0.8 mm, Graham Land 44 mm ± 8.8 mm, and Palmer Land 459 mm ± 91.8 mm to sea level, due to ice masses of 1569 Gt, 16,038 Gt and 166,263 Gt, respectively (Table 3). Alexander Island accounts for 32 mm ± 6.4 mm SLE, which is 70% of that from all surrounding islands (Table 3). On a glacier-by-glacier basis, the spatial pattern of potential SLE is similar to that within the region-by-region pattern but indicates heterogeneity (i) across Graham Land and across Alexander Island where in both cases the northern part has higher potential contributions than the southern part (Fig. 11B), and (ii) across Palmer Land where glaciers draining eastwards tend to have lower SLE than those draining westwards (Fig. 11B).

DISCUSSION

Our modelled ice thickness has the same 100 m spatial sampling as the model of Huss and Farinotti (2014) and resolves the same sort of rugged subglacial topography which is less well represented in the 1 km grid posting of Bedmap2 (Fretwell et al., 2013). Furthermore, our modelled ice thickness is more similar in planform distribution (Fig. 8) and in magnitude to that of Huss and Farinotti than to that of Bedmap2 (Figs. 5, 6, 7), which is remarkable given the far more sophisticated nature of the Huss and Farinotti (2014) model, and given the basis of Bedmap2 being OIB (2016) data. The discrepancy in magnitude of local (per grid cell) modelled ice thickness between this study, Bedmap2 (Fretwell et al., 2013) and Huss and Farinotti (2014) of up to 1000 m in some extreme cases (Fig. 9) contrasts with the generally good agreement in spatial pattern (Fig. 8). Thus whilst there is uncertainty in modelled ice thickness at any point, considerably so across Palmer Land, this uncertainty is apparently reduced by spatial averaging; specifically by consideration of glacier (catchment) volumes in preference to absolute ice thickness. Therefore with caution our model estimates of ice volume across Palmer Land can be combined with our estimates of ice volume for the northern parts of the Antarctic Peninsula and surrounding islands to give the first complete coverage assessment of ice volume and SLE contributions. Our use of the most recent distribution of CryoSat-2 data for parts of the Antarctic Peninsula mainland south of 70^{o}S has improved our knowledge of ice thickness, bed topography and SLE in that part of the Antarctic Peninsula.

Our discrimination of ice volume per major region quantifies the (i) dominance of western Palmer Land, which we propose contains 47 % of the total mainland ice volume (Table 3) and which is in agreement with the findings of Schannwell et al. (2018), (ii) importance of Alexander Island, which contains 70 % of the total ice volume on surrounding islands, and (iii) importance of the surrounding islands, which contain 12 % of all ice across the Antarctic Peninsula (Table 3). These quantifications are important because ‘mountain glacier and ice cap’ type glaciers have been highlighted as being especially vulnerable to climate change because they are relatively small and have relatively fast response times (Raper and Braithwaite, 2006; Meier et al., 2007). Furthermore glaciers on surrounding islands of the Antarctic Peninsula are situated at a lower elevation than those on the mainland and so are more susceptible not only to warming oceans (Meredith et al., 2005; Martinson et al., 2008; Schmidtko et al., 2014; Wouters et al., 2015; Cook et al. (2016) because the majority are tidewater glaciers (Davies et al., 2012), but also to warming air temperatures (Turner et al., 2012). Since 24 % of the mainland glaciers and 47 % of the surrounding island glaciers are below sea level (Table 3) they are

514 especially vulnerable to ice-shelf collapse in situations where they flow over retrograde slopes into ice
515 shelves (Scambos et al., 2003, 2014; Glasser et al., 2011; Rott et al., 2011).

516 The mountain glaciers on the surrounding islands have a total of 16,472 Gt ice mass with the capacity
517 to contribute 8 % of SLE from the Antarctic Peninsula, which is higher than 5 % suggested by the
518 Bedmap2 data (Table 3). The context of these figures is that previously it has been suggested that
519 mountain glaciers surrounding the Antarctic Peninsula account for 25 % of the total sea level rise
520 potential from glaciers and icecaps worldwide excluding the mainland Greenland and Antarctic
521 mainland ice sheet (Radic and Hock, 2010; Radic and Hock, 2011). For comparison, Pritchard and
522 Vaughan (2007) examined the northern Antarctic Peninsula between 64 °S to 70°S and suggested a
523 total SLE of 242 mm, which given that geographical extent excludes most of Palmer Land seems an
524 over-estimate given the 508 mm (± 101 mm) determined by this study for the whole mainland (Table
525 3). Bamber et al. (2009) also suggested that the Antarctic Peninsula has a SLE of 240 mm. For these
526 studies it is unclear exactly which glacier catchments were included and how these sea-level rise
527 figures were derived. Drewry (1983) and Heroy and Anderson (2005) suggested that the Antarctic
528 Peninsula and surrounding glaciers contain a SLE of 300 mm to 400 mm..
529
530 Our new estimates of the present ice volume, ice mass and SLE of the Antarctic Peninsula provide
531 context to contemporary observations of ice loss. Ivins et al. (2011) reported ice mass loss for the
532 northern Antarctic Peninsula (i.e. Graham Land) of 41.5 ± 9 Gt yr^{-1} between 2003 and 2009. For the
533 same time period, Gardner et al. (2013) reported ice mass loss for glaciers peripheral to the peninsula
534 and for islands surrounding the peninsula of 6 and 7 ± 4 Gt yr^{-1}, respectively. Considering the entirety
535 of the Antarctica Peninsula, Shepherd et al. (2012) have reported ice mass loss of 36 ± 10 Gt yr^{-1}
536 between 2005 and 2010. Rates of ice volume and ice mass change primarily between years 2003 and
537 2008 were reported by Scambos et al. (2014) of 27.7 ± 8.6 km^3 a^{-1} and 24.9 ± 7.8 Gt a^{-1}, equal to −0.73
538 m a^{-1} w.e. Sasgen et al., (2013) reported that the northern Antarctic Peninsula had mass loss −26 ± 3 Gt
539 yr^{-1} between 2003 and 2012. There is an obvious need for more field data to constrain both directly-
540 measured ice thickness, such as from ground penetrating radar and seismics, and also indirectly
541 estimated ice thickness changes (e.g. Carrivick et al., 2012). Notwithstanding the outstanding coverage
542 of the OIB data (2016) across the Antarctic Peninsula, directly measured distributed bed topography is
543 known from only a few small glaciers on James Ross Island (Engel et al., 2012; Fig. 3), and from Flask
544 Glacier and Starbuck Glacier on the Antarctic Peninsula mainland (Farinotti et al., 2013, 2014; Fig. 4).
545 Therefore the close analysis of ice thickness and volume on the surrounding islands that we have

provided is novel and of great utility for all concerned with present day glaciers and ongoing glacier changes. The circumstances for which this study's gridded ice thickness data across the mainland Antarctic Peninsula could most beneficially be used in partitioning volume, mass and melt water equivalent contributions under scenarios of changes in climate and oceanic forcing on the glacier systems.

CONCLUSIONS

We have modelled high-resolution (100 m grid) subglacial bed topography and distributed ice thickness across a far greater spatial extent than previously considered. We achieved this in a far simpler manner than previous efforts, requiring less input data and less parameterization. We have used the most-recent and best available DEMs. This approach has advantages, such as speed and coverage, and disadvantages, such as high uncertainty in at-a-point thickness. Specifically, we discriminate all glaciers of the mainland Antarctic Peninsula north of 74^{o}S and all glaciers on surrounding islands. We have reported ice thickness and bed elevation statistics, glacier volume and potential sea-level rise for each major mainland region and surrounding island group. It is important to make spatially-distributed discriminations because the Antarctic Peninsula spans several morpho-climatic zones.

Our comparison of model results highlights discrepancies between our modelled ice thickness, that of Bedmap2 (Fretwell et al., 2013) and that of Huss and Farinotti (2014). Our model is apparently able to reproduce the salient features of the rugged subglacial topography of the northern part of the Antarctic Peninsula (Trinity Peninsula, Graham Land and the surrounding islands) as well as total ice volume. In this study we have shown that if an emphasis is maintained on ice volume, and on ice thickness statistics per glacier rather than absolute ice thickness at-a-point, then a perfect plasticity type of model can be applied with caution to marine-terminating as well as land-terminating glaciers. Our ice thicknesses can be considered only as a first order estimate.

Our modelled ice thickness compares less favourably with that from previous efforts across Palmer Land. This is undoubtedly due to its poor treatment of very low gradient ice surfaces, but also perhaps a product of the newer CryoSat DEM that we have used for that region which is smoother than ASTER GDEM, for example. Recognizing that our model probably over-estimates ice thickness and hence volume, though not as much as Bedmap2, we suggest that western Palmer Land contains 41 % of the total ice volume of the Antarctic Peninsula. We have quantified that glaciers on surrounding islands

contain 12 % of all ice across the Antarctic Peninsula and of this Alexander Island contains 70 %. There are greater potential SLE contributions from glaciers on the eastern side of Graham Land than on the west and vice versa for Palmer Land. This asymmetry in SLE is interesting for considering atmospheric versus oceanic impacts on the Antarctic Peninsula glaciers.

The total ice mass on the Antarctic Peninsula is estimated to be 200,343 Gt, a SLE of 553 mm (± 110.6 mm), of which 8 % is contributed from glaciers on surrounding islands. Trinity Peninsula could contribute 4 mm ± 0.8 mm, Graham Land 44 mm ± 8.8 mm, and Palmer Land 459 mm ± 91.8 mm to sea level (Table 3). Across the entire Antarctic Peninsula, 24 % of the mainland ice and 47 % of ice on surrounding islands is below sea level, making these glaciers, especially those on Alexander Island and in western Palmer Land, extremely vulnerable to climate change as manifest in rising air and ocean temperatures.

Future development of the simple approach to estimating ice thickness and volume presented herein obviously needs to accommodate extensive shallow gradient ice surfaces. Other improvements could focus firstly on derivation of glacier flow lines using longitudinal flow stripes and lineations (e.g. Ely and Clark, 2016) rather than relying on relatively sparse centrelines. A representation of floating glacier terminii Could be made via a flotation criteria implemented at or close to the grounding line perhaps by using measured (or from the plastic model) elevation estimates to get a height above sea level and by assuming that ice thickness is equivalent to the thickness of the water column after accounting for density differences. A plastic model which does something similar, though in this case the ice surface is unknown, is in Gowan et al (2016).

REFERENCES

Bahr, D. B., Pfeffer, W. T. & Kaser, G. Glacier volume estimation as an ill-posed inversion. Journal of Glaciology 60, 922-934 (2014a).

Bahr, D. B., Pfeffer, W. T., & Kaser, G. A Review of Volume-Area Scaling of Glaciers. Reviews of Geophysics 53, 95-140 (2014b).

Bamber, J. L., Riva, R. E. M., Vermeersen, B. L. A. & Le Brocq, A. M., Reassessment of the potential sea-level rise from a collapse of the West Antarctic Ice Sheet. Science 324, 901-903 (2009).

Barrand, N.E., Hindmarsh, R.C., Arthern, R.J., Williams, C.R., Mouginot, J., Scheuchl, B., Rignot, E., Ligtenberg, S.R., Van Den Broeke, M.R., Edwards, T.L. & Cook, A.J. Computing the volume response of the Antarctic Peninsula ice sheet to warming scenarios to 2200. Journal of Glaciology 59, 397-409 (2013a).

612 Barrand, N.E., Vaughan, D.G., Steiner, N., Tedesco, M., Munneke, P.K., Van den Broeke, M.R. &
613 Hosking, J.S. Trends in Antarctic Peninsula surface melting conditions from observations and regional
614 climate modeling. Journal of Geophysical Research: Earth Surface 118, 315-330 (2013b).

615 Bindschadler, R., Choi, H., Wichlacz, A., Bingham, R., Bohlander, J., Brunt, K., Corr, H., Drews, R.,
616 Fricker, H., Hall, M. & Hindmarsh, R., 2011. Getting around Antarctica: new high-resolution mappings
617 of the grounded and freely-floating boundaries of the Antarctic ice sheet created for the International
618 Polar Year. The Cryosphere 5, 569–588.

619 Bliss, A. K., Hock, R., & Cogley, J.G. A new inventory of mountain glaciers and ice caps for the
620 Antarctic periphery. Annals of Glaciology 54, 191-199 (2013).

621 British Antarctic Survey. 2005. Antarctic Peninsula and Weddell Sea, 1:3,000,000 and 1:1,000,000
622 scale maps. BAS (Misc) 13A and 13B. Cambridge, British Antarctic Survey.

623 Cape, M.R., Vernet, M., Skvarca, P., Marinsek, S., Scambos, T. & Domack, E. Foehn winds link
624 climate-driven warming to ice shelf evolution in Antarctica. Journal of Geophysical Research:
625 Atmospheres, 120(21), (2015).

626 Carrivick, J.L., Davies, B.J., Glasser, N.F., Nývlt, D. & Hambrey, M.J., 2012. Late-Holocene changes
627 in character and behaviour of land-terminating glaciers on James Ross Island, Antarctica. Journal of
628 Glaciology, 58(212), pp.1176-1190.

629 Carrivick, J.L., Davies, B.J., James, W.H., Quincey, D.J. & Glasser, N.F., 2016. Distributed ice
630 thickness and glacier volume in southern South America. Global and Planetary Change, 146, pp.122-
631 132.

632 Cook, A. J. & Vaughan, D. G. Overview of areal changes of the ice shelves on the Antarctic Peninsula
633 over the past 50 years. The Cryosphere 4, 77-98 (2010).

634 Cook, A. J., Holland, P. R., Meredith, M. P., Murray, T., Luckman, A. & Vaughan, D. G. Ocean
635 forcing of glacier retreat in the western Antarctic Peninsula. Science 353, 283-286 (2016).

636 Cook, A. J., Fox, A. J., Vaughan, D. G. & Ferrigno, J. G. Retreating glacier fronts on the Antarctic
637 Peninsula over the past half-century. Science 308, 541-544 (2005).

638 Cook, A. J., Vaughan, D. G., Luckman, A. J. & Murray, T. A new Antarctic Peninsula glacier basin
639 inventory and observed area changes since the 1940s. Antarctic Science 26, 614-624 (2014).

640 Cook, A., Murray, T., Luckman, A., Vaughan, D., & Barrand, N., A new 100-m Digital Elevation
641 Model of the Antarctic Peninsula derived from ASTER Global DEM: methods and accuracy
642 assessment. Earth System Science Data 4, 129-142 (2012).

643 Davies, B. J., Carrivick, J. L., Glasser, N. F., Hambrey, M. J. & Smellie, J. L. Variable glacier response
644 to atmospheric warming, northern Antarctic Peninsula, 1988–2009. The Cryosphere 6, 1031-1048
645 (2012).

646 Davies, B.J., Golledge, N.R., Glasser, N.F., Carrivick, J.L., Ligtenberg, S.R., Barrand, N.E., Van Den
647 Broeke, M.R., Hambrey, M.J. & Smellie, J.L., 2014. Modelled glacier response to centennial
648 temperature and precipitation trends on the Antarctic Peninsula. Nature Climate Change 4, 993 (2014).

649 Depoorter, M.A., Bamber, J.L., Griggs, J.A., Lenaerts, J.T.M., Ligtenberg, S.R.M., Van den Broeke,
650 M.R. & Moholdt, G., Calving fluxes and basal melt rates of Antarctic ice shelves. Nature, 502, 89-92
651 (2013).

652 Domack, E. W. et al. (Eds.), Antarctic Peninsula Climate Variability: Historical and
653 Paleoenvironmental Perspectives, Washington, D.C., American Geophysical Union (Antarctic
654 Research Series, 79). 1-13.

655 Driedger, C., & Kennard, P.M. Glacier volume estimation on Cascade volcanoes: an analysis and
656 comparison with other methods. Ann. Glaciol., 8, 59-64 (1986a).

657 Driedger, C.L., & Kennard, P.M. Ice Volumes on Cascade Volcanoes: Mount Rainier, Mount Hood,
658 Three Sisters, and Mount Shasta Washington: U.S. Geological Survey Professional Paper, 1365
659 (1986b).

660 Drewry, D. J., Antarctic Ice Sheet - Aspects of Current Configuration and Flow. In. Gardner, R. &
661 Scoging, H. (Eds.) Mega-Geomorphology. British Geomorphological Research Group. Clarenden Press
662 pp. 18–38 (1983).

663 Ely, J.C. & Clark, C.D. Flow-stripes and foliations of the Antarctic ice sheet. Journal of Maps 12, 249-
664 259 (2016).

665 Engel, Z., Nývlt, D. & Láska, K. Ice thickness, areal and volumetric changes of Davies Dome and
666 Whisky Glacier in 1979-2006 (James Ross Island, Antarctic Peninsula). Journal of Glaciology 58, 904-
667 914 (2012).

668 Farinotti, D. & Huss, M. An upper-bound estimate for the accuracy of glacier volume–area scaling. The
669 Cryosphere, 7(6), 1707-1720 (2013).

670 Farinotti, D. et al. A method to estimate the ice volume and ice-thickness distribution of alpine glaciers.
671 Journal of Glaciology, 55(191), 422-430 (2009).

672 Farinotti, D., Corr, H. & Gudmundsson, G. H., The ice thickness distribution of Flask Glacier,
673 Antarctic Peninsula, determined by combining radio-echo soundings, surface velocity data and flow
674 modelling. Annals of Glaciology 54, 18-24 (2013).

675 Ferrigno, J. G. et al. Coastal-Change and Glaciological Map of the Trinity Peninsula Area and South
676 Shetland Islands, Antarctica: 1843-2001. USGS, Denver (2006).

677 Fischer, A. & Kuhn, M. Ground-penetrating radar measurements of 64 Austrian glaciers between 1995
678 and 2010. Annals of Glaciology, 54(64), 179-188 (2013).

679 Fretwell, L. O., et al. Bedmap2: improved ice bed, surface and thickness datasets for Antarctica. The
680 Cryosphere 7, 375-393 (2013).

681 Gardner, A.S., Moholdt, G., Cogley, J.G., Wouters, B., Arendt, A.A., Wahr, J., Berthier, E., Hock, R.,
682 Pfeffer, W.T., Kaser, G. & Ligtenberg, S.R. A reconciled estimate of glacier contributions to sea level
683 rise: 2003 to 2009. Science 340, 852-857 (2013).

684 Glasser, N. F., Scambos, T. A., Bohlander, J. A., Truffer, M., Pettit, E. C., & Davies, B. J. From ice-
685 shelf tributary to tidewater glacier: continued rapid glacier recession, acceleration and thinning of
686 Röhss Glacier following the 1995 collapse of the Prince Gustav Ice Shelf on the Antarctic Peninsula.
687 Journal of Glaciology 57, 397-406 (2011).

688 Golledge, N.R., Menviel, L., Carter, L., Fogwill, C.J., England, M.H., Cortese, G. & Levy, R.H.
689 Antarctic contribution to meltwater pulse 1A from reduced Southern Ocean overturning. Nature
690 Communications 5, 5107 (2014).

691 Golledge, N.R., Kowalewski, D.E., Naish, T.R., Levy, R.H., Fogwill, C.J. and Gasson, E.G.. The
692 multi-millennial Antarctic commitment to future sea-level rise. Nature 526 421 (2015).

693 Gowan, E.J., Tregoning, P., Purcell, A., Lea, J., Fransner, O.J., Noormets, R. and Dowdeswell, J.A.,.
694 ICESHEET 1.0: a program to produce paleo-ice sheet reconstructions with minimal assumptions.
695 Geoscientific Model Development 9, 1673-1682 (2016).

696 Heroy, D. C. & Anderson, J. B. Ice-sheet extent of the Antarctic Peninsula region during the Last
697 Glacial Maximum (LGM) - Insights from glacial geomorphology. GSA Bulletin 117, 1497-1512
698 (2005).

699 Hock, R., de Woul, M., Radic, V. & Dyurgerov, M. Mountain glaciers and ice caps around Antarctica
700 make a large sea-level rise contribution. Geophysical Research Letters 36, L07501 (2009).

701 Huber, J., Cook, A.J., Frank, P. and Zemp, M. A complete glacier inventory of the Antarctic Peninsula
702 based on Landsat 7 images from 2000 to 2002 and other preexisting data sets. Earth System Science
703 Data 9, 115 (2017).

704 Huss, M. & Farinotti, D. A high-resolution bedrock map for the Antarctic Peninsula. The Cryosphere 8,
705 1261-1273 (2014).

706 Hutchinson, M. A new procedure for gridding elevation and stream line data with automatic removal of
707 spurious pits. Journal of Hydrology, 106(3), pp.211-232 (1989).

708 Ivins, E. R., Watkins, M. M., Yuan, D.-N., Dietrich, R., Casassa, G. & Rülke, A., On-land ice loss and
709 glacial isostatic adjustment at the Drake Passage: 2003-2009. J. Geophys. Res. 116, B02403 (2011).

710 James, W. H. M. & Carrivick, J. L. Automated modelling of spatially-distributed glacier ice thickness
711 and volume. Computers & Geosciences 92, 90-103 (2016).

712 Kingslake, J., Ely, J.C., Das, I. & Bell, R.E. Widespread movement of meltwater onto and across
713 Antarctic ice shelves. Nature 544, 349 (2017).

714 Kunz, M. et al. Multi-decadal glacier surface lowering in the Antarctic Peninsula. Geophys. Res. Lett.
715 39, L19502 (2012).

716 Li, H. et al. An extended "perfect-plasticity" method for estimating ice thickness along the flow line of
717 mountain glaciers. Journal of Geophysical Research-Earth Surface, 117(F01020) (2012).

718 Linsbauer, A. et al. The Swiss Alps without glaciers – a GIS-based modelling approach for
719 reconstruction of glacier beds. In: Proceedings of Geomorphometry 2009, Zurich, Switzerland. (2009).

720 Linsbauer, A., Paul, F. & Haeberli, W. Modeling glacier thickness distribution and bed topography
721 over entire mountain ranges with GlabTop: Application of a fast and robust approach. Journal of
722 Geophysical Research, 117(F3) (2012).

723 Martinson, D. G. Stammerjohn, S. E. Iannuzzi, R. A. Smith, R. C. & Vernet, M. Deep-Sea Research
724 Part II -Topical Studies in Oceanography 55, 1964-1987 (2008).

725 Meier, M. F. et al. Glaciers dominate eustatic sea-level rise in the 21st century. Science, 317(5841),
726 1064-1067 (2007).

727 Meredith, M. P., & King, J. C. Rapid climate change in the ocean west of the Antarctic Peninsula
728 during the second half of the 20th century. Geophysical Research Letters, 32(19) (2005).

729 Morlighem, M., Rignot, E., Seroussi, H., Larour, E., Ben Dhia, H. and Aubry, D. A mass conservation
730 approach for mapping glacier ice thickness. Geophysical Research Letters 38 (2011).

731 Morris, E. M. & Vaughan, A. P. M. Spatial and temporal variation of surface temperature on the
732 Antarctic Peninsula and the limit of viability of ice shelves, in: Domack, E. W. et al. (Eds.), Antarctic

733 Peninsula climate variability: historical and palaeoenvironmental perspectives. American Geophysical
734 Union, Antarctic Research Series, Volume 79, Washington, D.C., pp. 61-68. (2003).

735 Nye, J. The flow of a glacier in a channel of rectangular, elliptic or parabolic cross-section. Journal of
736 Glaciology 5, 661-690 (1965).

737 Ó Cofaigh, C. et al. Reconstruction of ice-sheet changes in the Antarctic Peninsula since the Last
738 Glacial Maximum. Quaternary Science Reviews 100, 87-110 (2014).

739 Oliva, M., Navarro, F., Hrbáček, F., Hernández, A., Nývlt, D., Pereira, P., Ruiz-Fernández, J. & Trigo,
740 R. Recent regional climate cooling on the Antarctic Peninsula and associated impacts on the
741 cryosphere. Science of the Total Environment 580, 210-223 (2017).

742 Operation Ice-Bridge (2016) website: http://www.nasa.gov/mission_pages/icebridge/index.html last
743 visited May 2016.

744 Paolo, F.S., Fricker, H.A. & Padman, L. Volume loss from Antarctic ice shelves is accelerating.
745 *Science 348*, 327-331 (2015).

746 Pfeffer, W. T. et al. The Randolph Glacier Inventory: a globally complete inventory of glaciers. Journal
747 of Glaciology, 60(221), 537-552 (2014).

748 Pritchard, H. D. & Vaughan, D. G. Widespread acceleration of tidewater glaciers on the Antarctic
749 Peninsula. Journal of Geophysical Research-Earth Surface 112, F03S29, 01-10 (2007).

750 Pritchard, H. D., Arthern, R. J., Vaughan, D. G., & Edwards, L. A. Extensive dynamic thinning on the
751 margins of the Greenland and Antarctic ice sheets. Nature 461, 971-975 (2009).

752 Pritchard, H., Ligtenberg, S.R.M., Fricker, H.A., Vaughan, D.G., Van den Broeke, M.R. & Padman, L..
753 Antarctic ice-sheet loss driven by basal melting of ice shelves. Nature, 484(7395), 502 (2012).

754 Radić, V. & Hock, R. Regional and global volumes of glaciers derived from statistical upscaling of
755 glacier inventory data. Journal of Geophysical Research: Earth Surface 115, F01010 (2010).

756 Radic, V. & Hock, R. Regionally differentiated contribution of mountain glaciers and ice caps to future
757 sea-level rise. Nature Geosci 4, 91-94 (2011).

758 Raper, S. C., & Braithwaite, R. J. Low sea-level rise projections from mountain glaciers and icecaps
759 under global warming. Nature, 439(7074), 311-313 (2006).

760 Rignot, E., Mouginot, J. & Scheuchl, B. Ice flow of the Antarctic ice sheet. Science, 333(6048), 1427-
761 1430 (2011).

762 Rignot, E., Jacobs, S., Mouginot, J., & Scheuchl, B. Ice-shelf melting around Antarctica. Science,
763 341(6143), 266-270 (2013).

764 Rott, H., Müller, F. & Floricioiu, D. The imbalance of glaciers after disintegration of Larsen B ice
765 shelf, Antarctic Peninsula. The Cryosphere 5, 125-134 (2011).

766 Sasgen, I., Konrad, H., Ivins, E.R., Van den Broeke, M.R., Bamber, J.L., Martinec, Z. & Klemann, V..
767 Antarctic ice-mass balance 2003 to 2012: regional reanalysis of GRACE satellite gravimetry
768 measurements with improved estimate of glacial-isostatic adjustment based on GPS uplift rates. The
769 Cryosphere 7, 1499-1512 (2013).

770 Scambos, T., Hulbe, C. & Fahnestock, M. Climate-induced ice shelf disintegration in the Antarctic
771 Peninsula, in: Domack, E.W. et al. (Eds.), Antarctic Peninsula climate variability: historical and
772 palaeoenvironmental perspectives. American Geophysical Union, Antarctic Research Series, Volume
773 79, Washington, D.C., pp. 79-92 (2003).

Scambos, T.A., Berthier, E., Haran, T., Shuman, C.A., Cook, A.J., Ligtenberg, S. & Bohlander, J.. Detailed ice loss pattern in the northern Antarctic Peninsula: widespread decline driven by ice front retreats. The Cryosphere 8, 2135-2145 (2014).

Schannwell, C., Cornford, S., Pollard, D. & Barrand, N.E. Dynamic response of Antarctic Peninsula Ice Sheet to potential collapse of Larsen C and George VI ice shelves. The Cryosphere 12, 2307-2326 (2018).

Schoof, C. Ice sheet grounding line dynamics: Steady states, stability, and hysteresis. Journal of Geophysical Research: Earth Surface 112 (2007).

Shepherd, A., Ivins, E.R., Geruo, A., Barletta, V.R., Bentley, M.J., Bettadpur, S., Briggs, K.H., Bromwich, D.H., Forsberg, R., Galin, N. & Horwath, M. A reconciled estimate of ice-sheet mass balance. Science 338, 1183-1189 (2012).

Schmidtko, S., Heywood, K. J., Thompson, A. F. & Aoki, S. Science 346, 1227-1231 (2014).

Skvarca, P. & De Angelis, H. Impact assessment of regional climatic warming on glaciers and ice shelves of the northeastern Antarctic Peninsula, in: Domack, E.W., et al. (Eds.), Antarctic Peninsula climate variability: historical and palaeoenvironmental perspectives. American Geophysical Union, Antarctic Research Series, Volume 79, Washington, D.C., pp. 69-78 (2003).

Turner, J., Lu, H., White, I., King, J.C., Phillips, T., Hosking, J.S., Bracegirdle, T.J., Marshall, G.J., Mulvaney, R. & Deb, P. Absence of 21st century warming on Antarctic Peninsula consistent with natural variability. Nature 535, 411 (2016).

Turner, J. et al. Antarctic climate change and the environment: an update. Polar Record 50, 237-259 (2013).

Turner, J. et al., Antarctic Climate Change and the Environment. Scientific Committee on Antarctic Research, Cambridge (2009).

van den Broeke, M. Strong surface melting preceded collapse of Antarctic Peninsula ice shelf. Geophysical Research Letters, 32(12), (2005).

Van Wessem, J.M., Ligtenberg, S., Reijmer, C.H., Van De Berg, W.J., Van Den Broeke, M.R., Barrand, N.E., Thomas, E.R., Turner, J., Wuite, J., Scambos, T.A. & Van Meijgaard, E.. The modelled surface mass balance of the Antarctic Peninsula at 5.5 km horizontal resolution. The Cryosphere 10, 271-285 (2016).

Vieli, A. & Nick, F.M., 2011. Understanding and modelling rapid dynamic changes of tidewater outlet glaciers: issues and implications. Surveys in Geophysics 32, 437-458 (2011).

Wouters, B., Martin-Español, A., Helm, V., Flament, T., van Wessem, J.M., Ligtenberg, S.R., Van den Broeke, M.R. & Bamber, J.L. Dynamic thinning of glaciers on the Southern Antarctic Peninsula. Science 348, 899-903 (2015).

Zekollari, H., & Huybrechts, P. On the climate-geometry imbalance, response time and volume-area scaling of an alpine glacier: insights from a 3-D flow model applied to Vadret da Morteratsch, Switzerland. Annals of Glaciology 56, 51-62 (2015).

ACKNOWLEDGEMENTS

Development of the perfect plasticity model was supported by a NERC PhD studentship (NE/K500847/1) to WJ. Alison Cook provided the DEM and the glacier outlines for areas north of 70°S. We thanks the Bedmap2 team for their publically-available data. We thank Matthias Huss and Daniel Farinotti for their data made available via their supplementary information.

TABLES

Mainland Antarctic Peninsula	
TP-West	Trinity Peninsula west of main divide
TP-East	Trinity Peninsula east of main divide
GL-West	Graham Land west of main divide
GL-East	Graham Land east of main divide
PL-west	Palmer Land west of main divide
PL-east	Palmer Land east of main divide
Surrounding Islands	
N	Andersson, Bransfield, Dundee, Joinville, Jonasson, D'Urville
N-west	South Shetland Islands, Deception, Low, Smith, Snow
N-east	James Ross, Eagle, Lockyer, Snow Hill, Vega
C-west	Adelaide, Anvers, Astrolabe, Belding, Brabant, Butler, Christiana, Dubois, Hoseason, Horseshoe, Krogh, Larrouy, Lavoisier, Liard, Liege, Millerand, Pitt, Pourquois Pass, Rabot, Renaud, Tower, Trinity, Two Hummock, Watkins, Wiencke
C-east	Dollerman, Ewing, Francis, Gipps, Hearst, Robertson, Seal Nunataks, Steele, Tonkin
S-west	Case, Charcot, DeAtley, Dorsey, Eklund Islands, Latady, Rothschild, Smyley, Spaatz
A	Alexander Island

Table 1. Explanation of geographical codes and groupings of major glacier regions for the Antarctic Peninsula and surrounding islands used in this study.

	This study		**Bedmap2 (Fretwell et al., 2013)**		**Huss and Farinotti (2014)**	
Region	Mean ice thickness (m)	Maximum ice thickness (m)	Mean ice thickness (m)	Maximum ice thickness (m)	Mean ice thickness (m)	Maximum ice thickness (m)
Mainland						
TP-West	459	1457	187	484	277	1075
TP-East	423	1577	141	521	260	1080
GL-West	373	2216	130	985	251	1316
GL-East	563	2136	223	1291	354	1983
PL-west	1305	2668	892	2451		
PL-east	571	2521	937	3171	370*	1835*
Surrounding islands						
N	480	1603	227	477	256	656
N-west	242	1113	56	391		
N-east	335	1719	116	436	234	920
C-west	516	1914	184	738	228	1159
C-east	385	1594	258	435	14*	605*
S-west	397	2166	326	589		
A	569	2304	323	1640		

*These values of Huss and Farinotti's dataset only include calculations covering a small part of these regions.

Table 2: Comparison of mean and maximum ice thickness per major region as modelled by this study, Bedmap2 (Fretwell et al., 2013) and Huss and Farinotti (2014). All ice thickness estimates have a worst-case uncertainty of ± 31 %.

Region	This study				Bedmap2 (Fretwell et al., 2013)			Huss and Farinotti (2014)		
	Ice volume (km^3)	Ice volume < 0 m.asl (km^3)	Ice mass (Gt)	Sea level equivalent (mm)	Ice volume (km^3)	Ice volume < 0 m.asl (km^3)	Sea level equivalent (mm)	Ice volume (km^3)	Ice volume < 0 m.asl (km^3)	Sea level equivalent (mm)
TP-west	1,211	282	791	2	494	13	2	745	41	2
TP-east	1,362	449	778	2	494	13	2	929	160	2
GL-west	8,843	1,639	6,138	17	3,070	69	10	5,972	639	13
GL-east	16,208	4,588	9,900	27	6,441	896	18	10,275	2,111	19
PL-west	122,772	34,013	75,623	209	117,224	21,331	311			
PL-east	109,810	3,424	90,641	250	197,225	82,130	373			
sum mainland	260,207	44,395	183,871	508	324,948	104,452	715	17,922	2,951	35
N	1,121	541	493	1	539	122	1	625	149	1
N-west	663	208	387	1	146	6	0			
N-east	662	138	447	1	253	18	1	583	155	1
C-west	4,003	1,794	1,881	5	1,571	176	5	2,047	228	4
C-east	717	284	369	1	553	168	1			
S-west	2,529	1,091	1,224	3	4,373	1,374	10			
A	27,078	13,380	11,671	32	15,324	3,916	37			
sum islands	36,772	17,436	16,472	46	22,760	5,778	55	3,255	533	6
sum total	296,979	61,831	200,343	553	347,708	110,231	770	21,177	3,484	42

Table 3. Summary per major mainland and surrounding island region of total ice volume, ice volume below sea level and maximum potential sea-level equivalent (SLE) according to the modelling of this study, Bedmap2 (Fretwell et al., 2013) data, and the modelling of Huss and Farinotti (2014). All volumes and sea level equivalent estimates have a worst-case uncertainty of ± 20 %.

FIGURES

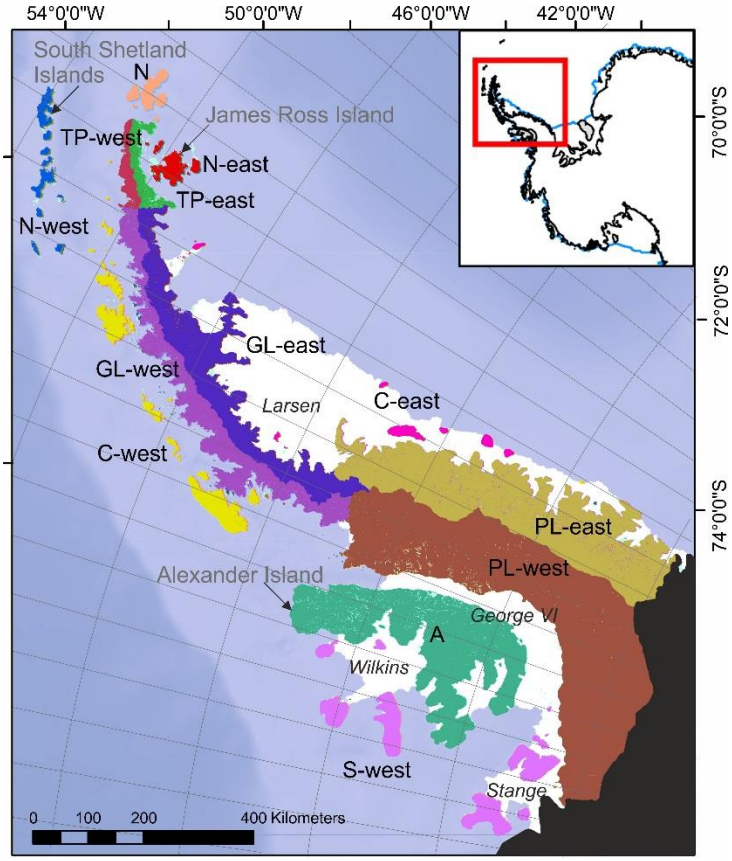

Figure 1. Major glacier regions across the Antarctic Peninsula as used in this study to spatially discriminate ice thickness, bed topography, ice volume and potential sea level contributions. Surrounding islands are grouped spatially and the labelled codes for these groups are expanded in Table 1.

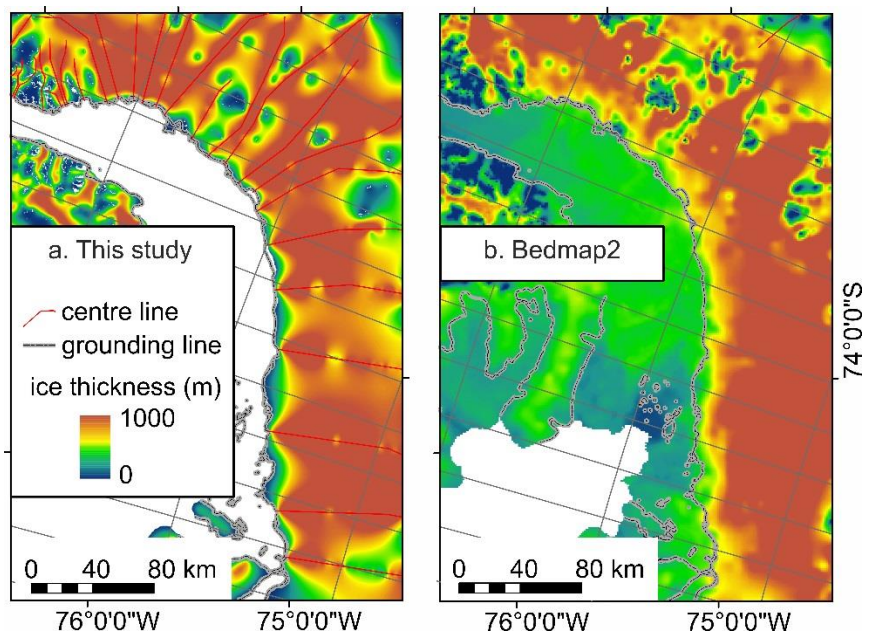

Figure 2. Example of multiple centrelines per single glacier outline artificially introduced to accommodate application of the VOLTA model to wide, low-angle and coalescing glaciers that are typical of the southern part of the Antarctic Peninsula, in this case on the mainland opposite the south coast of Alexander Island. The resultant VOLTA-computed ice thickness (A) matches the magnitude and spatial pattern of ice thickness from Bedmap2 (B) well. Grounding lines are from Rignot et al. (2011). Bedmap2 data is from Fretwell et al. (2013).

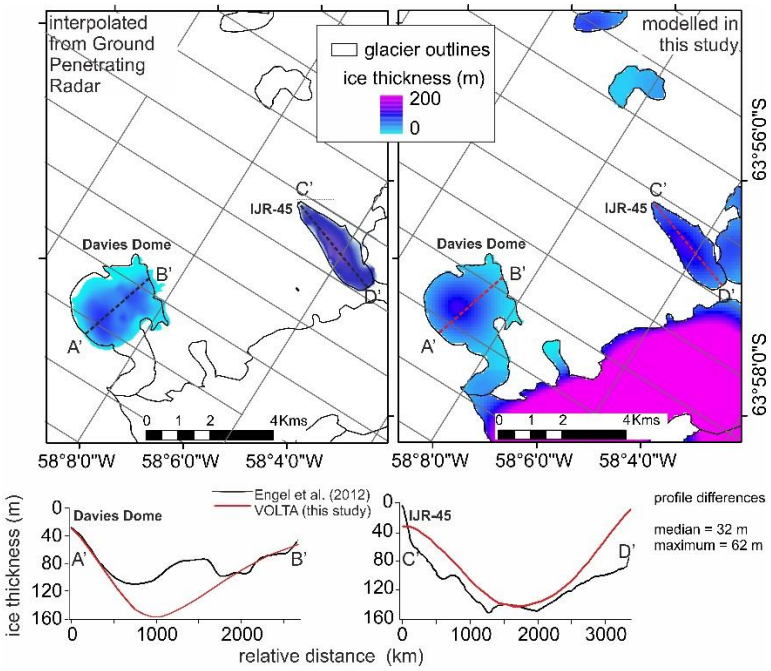

Figure 3. Comparison of ice thickness modelled in this study with that from Engel et al. (2012) who interpolated between ground penetrating radar data on Davies Dome ice cap and IJR-45 valley glacier, both on the Ulu Peninsula on James Ross Island. The ice thickness transects are chosen to closely follow GPR lines so as to exclude interpolation error from these transect comparisons.

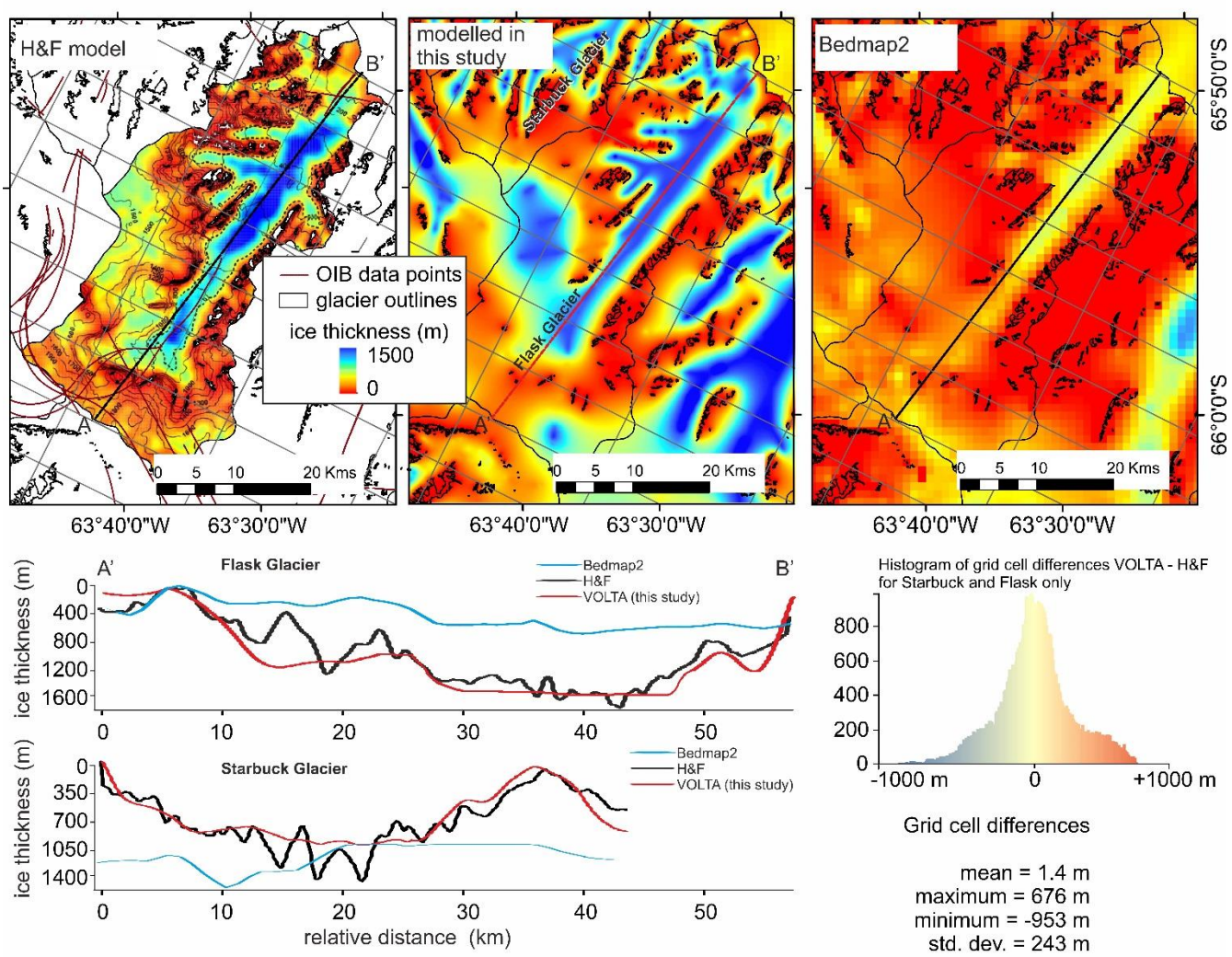

Figure 4. Comparison of ice thickness modelled in this study with that from Farinotti et al. (2013, 2014) who optimised their ice thickness model using ground penetrating radar data and ice velocity data on Flask Glacier and on Starbuck Glacier, both of which are tidewater glaciers. The glacier outline at the end of the transect and at point B' is determined by the grounding line, as mapped by Rignot et al. (2011).

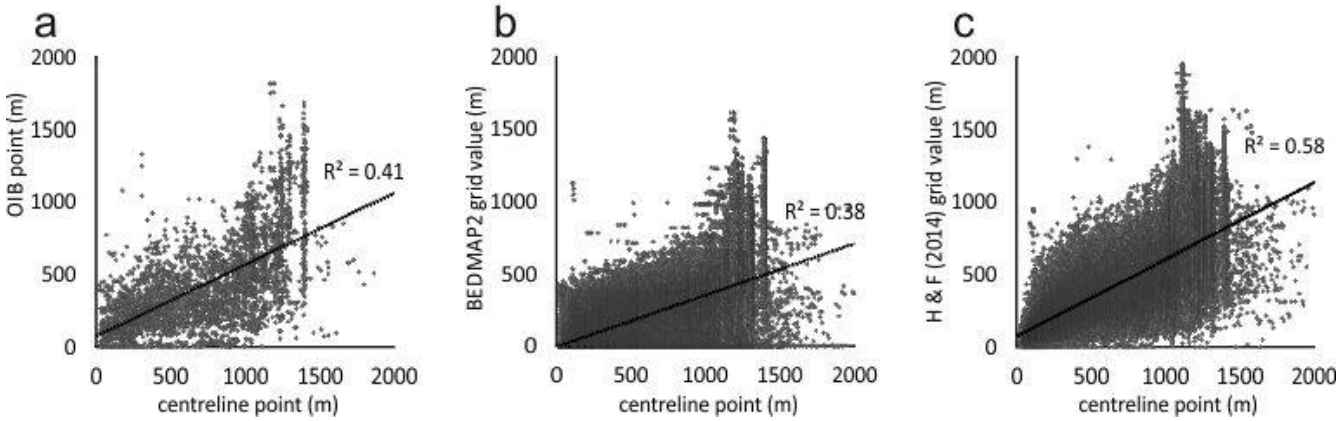

Figure 5. Cross-over analysis of ice thickness for our modelled glacier centreline points (n = 81,463) and closest (if within 500 m) Operation Ice-Bridge (2016) points (a). For comparison, the corresponding ice thickness grid cell values of Bedmap2 (Fretwell et al., 2013) ice thickness and Huss and Farinotti's (2014) ('H&F') ice thickness at each of these centreline points are also shown in panels b and c, respectively.

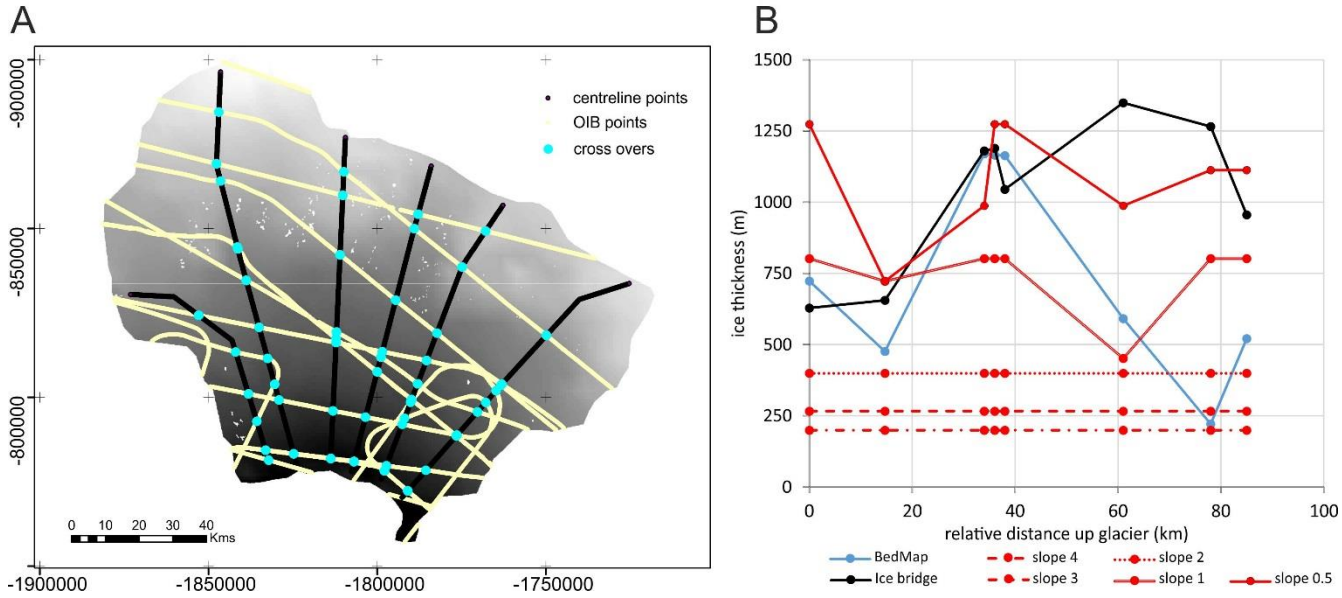

Figure 6. Cross-over analysis of ice thickness for our modelled glacier centreline points on the largest (area) single glacier in Palmer Land (A) illustrating the very low slope threshold values needed to generate an ice thickness estimate with a perfect plasticity model and the unrealistic nature of these estimates (B).

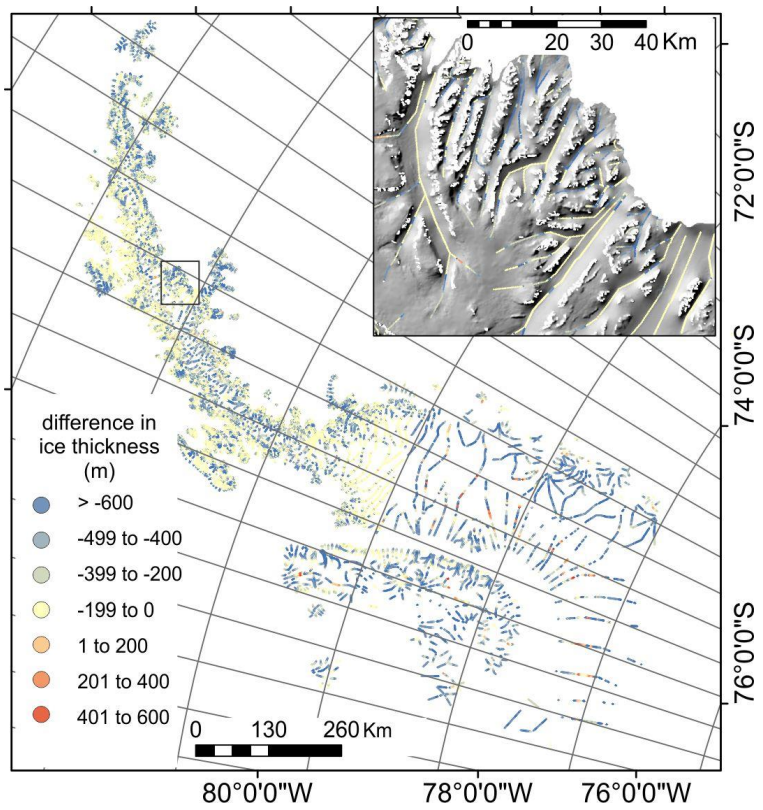

Figure 7. Spatial pattern of difference of ice thickness modelled on centreline points in this study with the nearest (if within 500 m) Operation Ice-Bridge (2016) ice thickness point. Inset is chosen to be same area as emphasized by Huss and Farinotti (2014) for its subglacial trough topography.

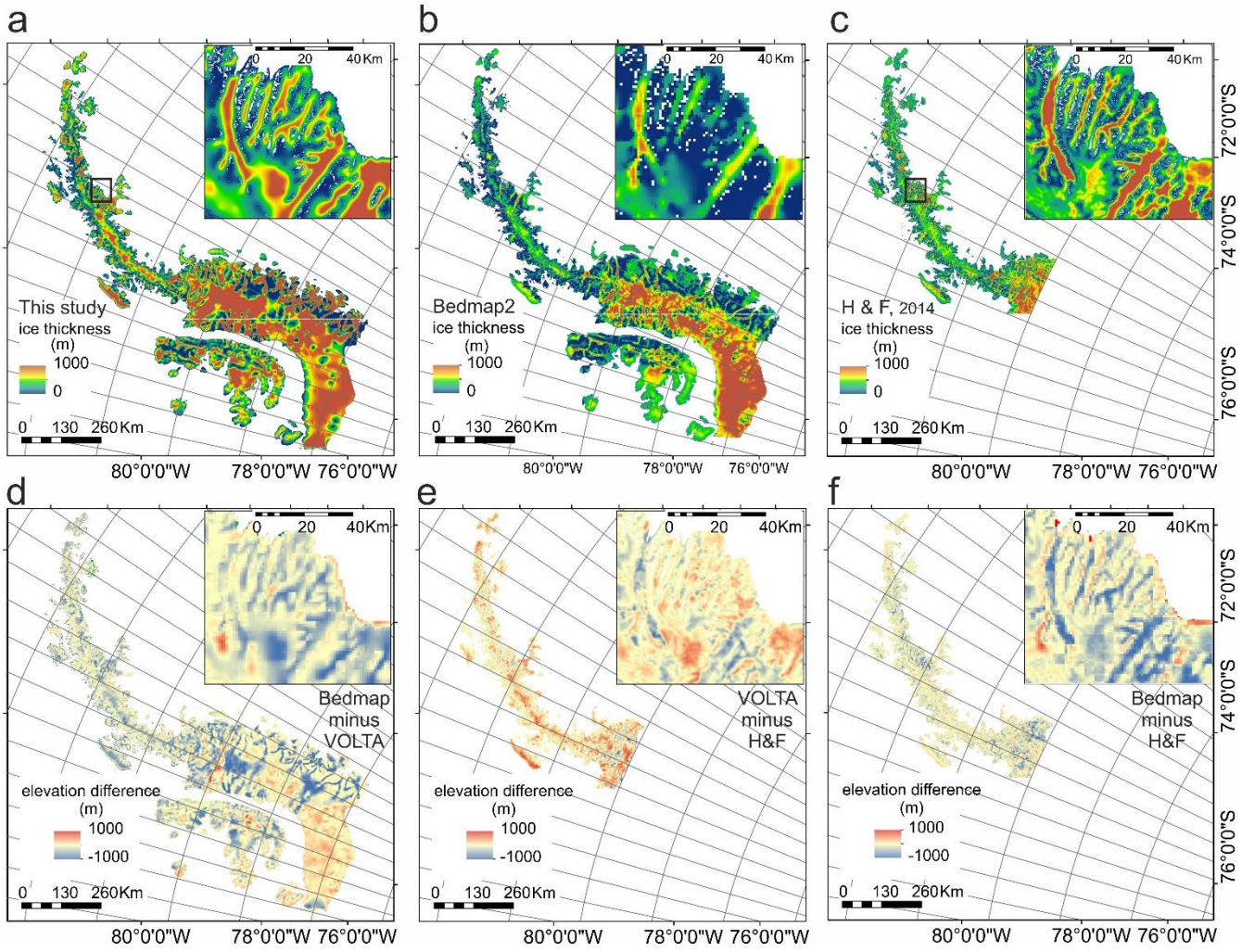

Figure 8. Gridded ice thickness modelled in this study (a) the Bedmap2 (Fretwell et al., 2013) dataset (b), and modelled by Huss and Farinotti (2014) ('H&F') (c). Differences in ice thickness between Bedmap2 and this study, between Huss and Farinotti and this study, and between Huss and Farinotti and Bedmap2 are shown in panels d, e and f, respectively. Colour scales are identical in all panels and in all insets. Inset is chosen to be same area as emphasised by Huss and Farinotti for its subglacial trough topography.

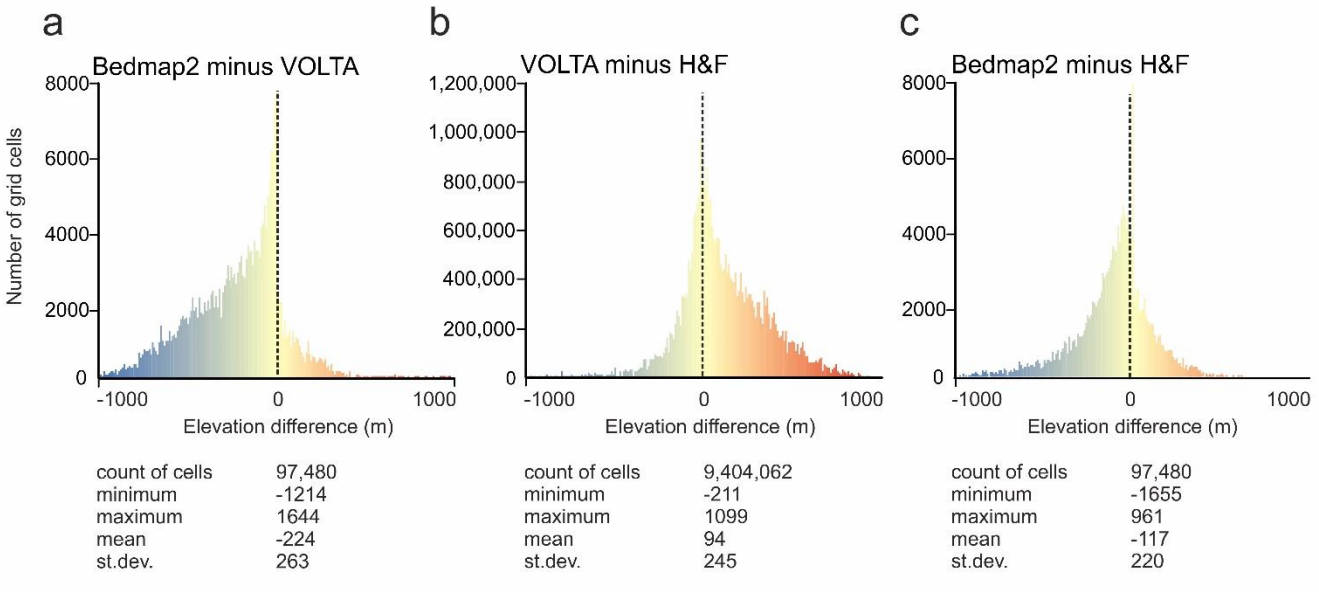

Figure 9. Histogram comparison of grid cell values between the modelled ice thickness of this study and Bedmap2 (a), between this study and the ice thickness modelled by Huss and Farinotti (2014) ('H&F') (b) and Huss and Farinotti and Bedmap2 (c). Bars are coloured to match the elevation differences as mapped in Figure 4.

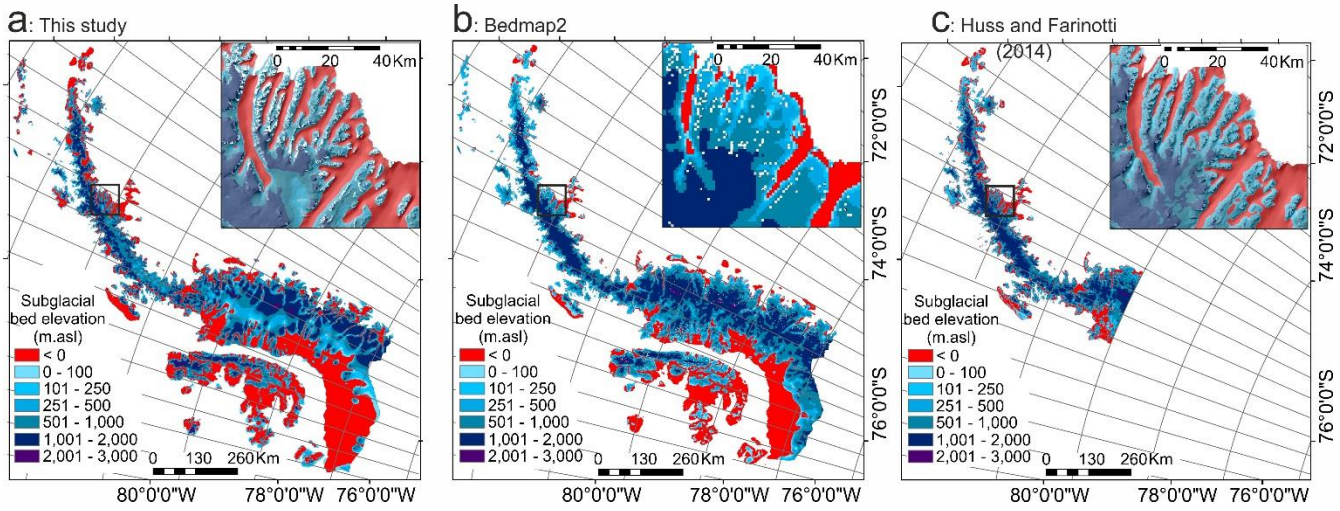

Figure 10. Subglacial topography, emphasizing those areas of the Antarctic Peninsula that are below sea level and so potentially contribute by a relatively small amount to sea-level rise, as modelled by this study (a) within the Bedmap2 (Fretwell et al., 2013) dataset (b) and as modelled by Huss and Farinotti (2014) (c). Note that the insets in panels a and b are underlain by hillshaded bed topography for clarity of the 100 m resolution grid.

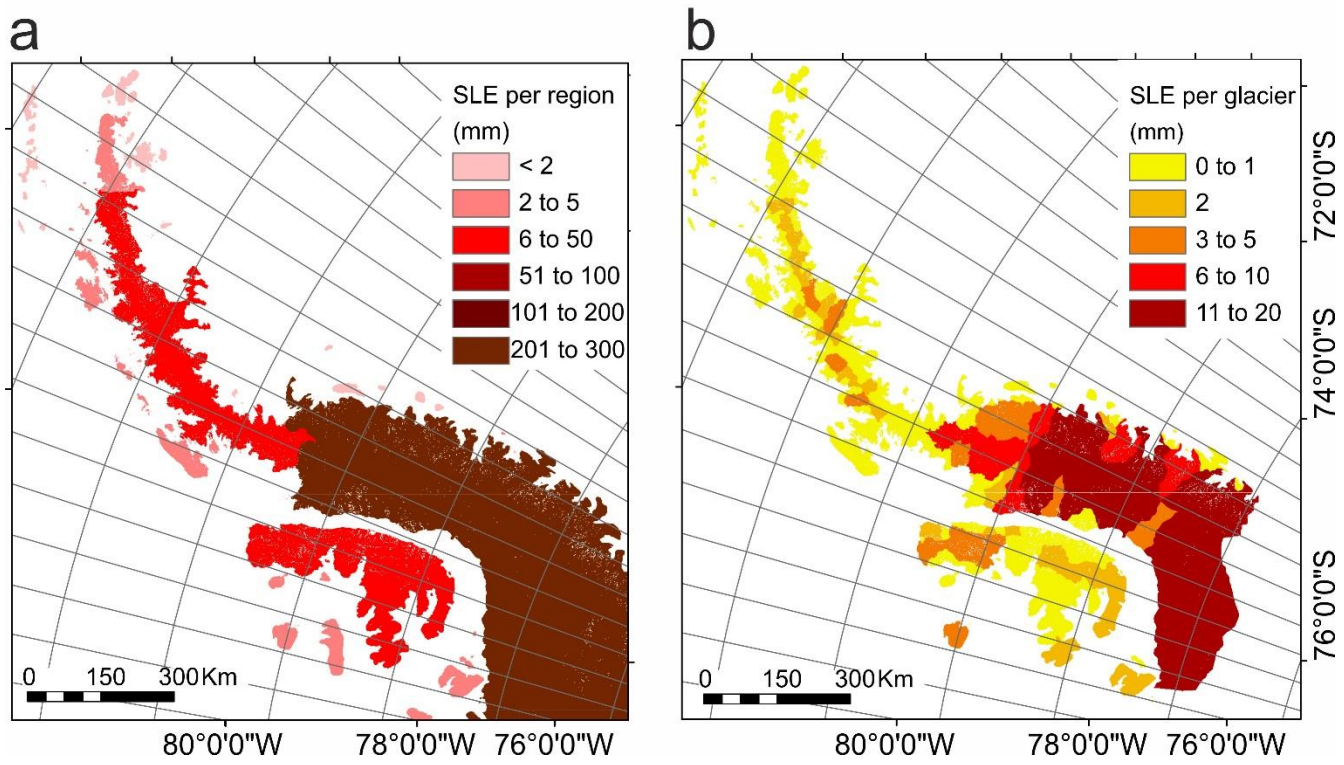

1002

1003 **Figure 11.** Maximum potential sea-level equivalent (SLE) contributions spatially discriminated per
1004 major region (a) and per glacier (b). Note the colour scales are different between the two panels.